Eur. Phys. J. C (2026) 86:677
https://doi.org/10.1140/epjc/s10052-026-15894-8

THE EUROPEAN PHYSICAL JOURNAL C

Regular Article - Theoretical Physics

Bound on Lyapunov exponents with spinning particles in Kerr–Newman spacetimes

Chuang Yang[1,a], **Chuanhong Gao**[2,b], **Deyou Chen**[1,3,c], **Kangqiao Liu**[1,3,d]

[1] School of Science, Xihua University, Chengdu 610039, China
[2] Sichuan Technology and Business University, Chengdu 611754, China
[3] Key Laboratory of High Performance Scientific Computation, Xihua University, Chengdu 610039, China

Received: 23 March 2026 / Accepted: 25 May 2026

Abstract In this work, we investigate the Lyapunov exponents associated with the chaotic dynamics of spinning charged particles in the Kerr–Newman spacetime, focusing on whether these exponents can exceed the MSS scale. The black hole charge is held fixed, and two distinct configurations are analyzed: the black hole rotation aligned and anti-aligned with the z-axis. In the aligned case, an exceedance occurs exclusively when the black hole angular momentum surpasses a critical threshold; notably, for a fixed angular momentum of 0.20, no exceedance is observed irrespective of variations in the particle's spin, charge, or total angular momentum. In the anti-aligned configuration, by contrast, exceedances emerge once the black hole angular momentum, or the particle's spin, charge, or total angular momentum exceeds its respective threshold. Furthermore, an increase in the particle's negative charge suppresses chaotic motion, whereas an increase in positive charge enhances it. In the extremal limit, the black hole reduces to a zero-temperature system, wherein the exponents remain strictly positive for all spin configurations. These results show that these exponents associated with chaotic dynamics can be larger than the MSS scale.

Contents

[a] e-mail: chuangyangyc@hotmail.com
[b] e-mail: chuanhonggao@hotmail.com
[c] e-mail: deyouchen@hotmail.com (corresponding author)
[d] e-mail: kqliu@xhu.edu.cn

1 Introduction

Chaos is a ubiquitous nonlinear phenomenon in nature, which is fundamentally characterized by an extreme sensitivity to initial conditions in dynamical systems. In classical systems, trajectories of dynamics exhibit a sensitive dependence on the initial conditions. Specifically, a small change in the initial conditions causes the trajectories to deviate exponentially from their initial positions. This sensitivity is quantified by a Lyapunov exponent (LE), which is defined as [1]

$$\lambda_c = \lim_{t\to\infty} \lim_{x_0\to 0} \frac{1}{t} ln \left| \frac{\Delta x(t)}{\Delta x_0} \right|, \tag{1.1}$$

where $\Delta x(t)$ and Δx_0 denote the differences between two trajectories at an arbitrary time t and the initial time, respectively. A positive value of $\lambda_c > 0$ indicates that the system is chaotic. Chaos also exists in quantum systems. However, owing to the non-smooth structure of the phase space in the quantum regime, the notion of classical trajectories is not directly applicable, thereby precluding a definition of chaos based on trajectory divergence as in classical systems. To circumvent this difficulty, a variety of diagnostic tools have been developed for the study of quantum chaos, including the Loschmidt echo [2], out-of-time-order correlators (OTOCs) [3–5] and Krylov complexities [6]. The OTOCs, $F(t,\vec{x}) = \langle V(0)W(t,\vec{x})V(0)W(t,\vec{x})\rangle$, serve as key tools for diagnosing quantum information scrambling [7]. In holographic systems at finite temperature, the OTOC has a simple

Published online: 22 June 2026

form [8]

$$\frac{\langle V(0)W(t,\vec{x})V(0)W(t,\vec{x})\rangle}{\langle V(0)V(0)\rangle\langle W(t,\vec{x})W(t,\vec{x})\rangle} = 1-\varepsilon_{\Delta_V\Delta_W} exp\left[\lambda_q\left(t-t_\star-\frac{|\vec{x}|}{v_B}\right)\right], \tag{1.2}$$

where $\varepsilon_{\Delta_V\Delta_W}$ is a multiplicative factor and contains information about the operators V and W, λ_q is a LE, $t_\star$ is a scrambling time, and v_B is a butterfly velocity. However, it has been found that OTOCs can misclassify quantized integrable systems as chaotic, thereby violating the expected correspondence between classical and quantum chaos [9,10]. To rectify this flaw in the definition of quantum chaos, Trunin introduced the logarithmic OTOC and reformulated the LE [11]. This refined definition ensures a direct correspondence between classical and quantum chaos.

Recently, Maldacena, Shenker, and Stanford (MSS) put forward a seminal conjecture that in thermal quantum systems with a large number of degrees of freedom, the LE is subject to a universal upper bound governed by the system temperature T, namely [12]

$$\lambda_q \leq \frac{2\pi T}{\hbar}. \tag{1.3}$$

This work uncovers the ultimate rate of information scrambling in chaotic systems and establishes a fundamental connection between gravity and chaotic dynamics through the AdS/CFT correspondence [13,14]. Since its proposal, this groundbreaking conjecture has rapidly garnered widespread attention. The saturation of the chaos bound in the Sachdev–Ye–Kitaev (SYK) model provides strong support for this work [15–18]. In addition, quantum chaotic behavior has also been studied in the Bose–Fermi Kondo model [19]. Related research has also been further extended in chaotic phenomena in holographic duality [20] and maximally chaotic quantum systems [21]. For a single-particle system, considering that a particle moves radially and is close to a black hole (BH) by a strong enough external forces without falling into it, Hashimoto and Tanahashi found that the exponent is not related to the species and strength of the forces [22], but only to the surface gravity of the BH, namely

$$\lambda_c \leq \kappa, \tag{1.4}$$

where κ is the surface gravity. From the relation between the surface gravity and temperature, this result is completely consistent with Eq. (1.3).

However, subsequent studies have shown that LEs can exceed the surface gravity in various spacetimes, which implies that these exponents are larger than the MSS scale. The exponents characterizing the chaotic motion of charged particles around charged BHs were investigated by Zhao et al. using the near-horizon expansion method [23]. The phenomenon of the exponents exceeding the surface gravity was observed in the near-horizon regions of certain BHs, whereas no such behavior was found near the horizons of Reissner–Nordström (RN) and Reissner–Nordström anti-de Sitter (RN-AdS) BHs. In the aforementioned study, the angular momenta of the particles were not taken into account. Upon incorporating this contribution, the phenomenon was found not only in RN and RN-AdS spacetimes [24], but also in other spherically symmetric spacetimes [25–32] and rotating spacetimes, such as Kerr–Newman [33], Kerr–Newman–dS [34], Kerr–Newman–AdS [35] and Kerr–Sen–AdS spacetimes [36]. The angular momentum ranges and parameter regimes associated with this phenomenon have also been identified [37]. When quantum gravitational corrections are incorporated into the framework, the momentum operator undergoes appropriate modifications; despite these adjustments, the phenomenon persists across all tested parameter regimes [38,39]. While these phenomena were initially discovered in classical systems, analogous behavior also manifests in quantum systems. For instance, in the closed string system in AdS spacetime, the exponent assumes a modified form related to the string's winding number [40]. Hashimoto and Sugiura, employing a reparameterization-independent approach, demonstrated that the universal bound imposed by causality can be surpassed for certain potential functions [41]. This phenomenon also manifests in BTZ spacetime [42–44]; however, it can not occur when one introduces an effective temperature In the analysis.

Recently, the exponents of spinning particles in RN spacetime have been investigated, and the results reveal that these exponents can likewise exceed the surface gravity of the RN BH [45]. In that work, the BH charge plays a pivotal role: when the charge is sufficiently large, even particles with moderate angular momentum and spin can give rise to the exponents that surpass the surface gravity; conversely, for small charges, no such exceedance occurs regardless of variations in the particle's spin or angular momentum. However, this study is restricted to spherically symmetric spacetimes with non-zero temperature. To the best of our knowledge, investigations into the upper bound of these exponents for spinning particles in axisymmetric spacetimes remain notably scarce, particularly in zero-temperature systems.

In this work, we investigate the relationship between the LEs associated with the chaotic dynamics of spinning particles in Kerr–Newman spacetime and the surface gravity, with the aim of examining their relation to the MSS scale. While numerous studies have delved into the spin dynamics of particles in Kerr–Newman spacetime [46–48], research on their chaotic motion and the corresponding LEs is notably limited. We focus on the impacts of the BH angular momentum, the particle angular momentum, the particle spin, and its charge on the exponents. When the BH reaches extremality, it transforms into a zero-temperature system. Such systems, for instance, BHs in AdS spacetime, correspond to the ground state or low-energy limit of conformal field theories. By exploring the chaotic properties of these systems, we can rigorously test the universality of the holographic duality principle. In string theory, extremal BHs are dual to BPS states, with their entropy and dynamics directly linked to microscopic degrees of freedom. The explicit behavior of the exponents in extremal BHs may unveil profound connections between information conservation and chaos in quantum gravity. Consequently, we extend our analysis to extremal Kerr–Newman, RN and Kerr spacetimes.

The rest of the paper is organized as follows. In Sect. 2, we review the motions of the spinning particles in the Kerr–Newman spacetime. In Sect. 3, we analyze the dependence of the LEs on the BH angular momentum, the particle's total angular momentum, the magnitude and orientation of the spin, and the charge, and explicitly verify the upper bound of these exponents in both non-extremal and extremal Kerr–Newman spacetimes. The final section presents our conclusions and discussions.

2 Motions of spinning particles in Kerr–Newman spacetimes

The Kerr–Newman BH describes a stationary, axisymmetric spacetime and represents an exact solution to the Einstein–Maxwell equations in the presence of both rotation and electric charge. In Boyer–Lindquist coordinates, its metric is given by

$$ds^2 = -\frac{\Delta}{\Sigma}\left(dt - a\sin^2\theta\, d\phi\right)^2 + \frac{\Sigma}{\Delta}dr^2 + \Sigma\, d\theta^2 + \frac{\sin^2\theta}{\Sigma}\left(a\, dt - (r^2+a^2)\, d\phi\right)^2, \tag{2.1}$$

with an electromagnetic potential

$$A = A_\mu dx^\mu = -\frac{Qr}{\Sigma}\left(dt - a\sin^2 d\phi\right), \tag{2.2}$$

where

$$\Delta = r^2 - 2Mr + a^2 + Q^2, \quad \Sigma = r^2 + a^2\cos^2\theta. \tag{2.3}$$

The parameters M, a and Q denote the mass, rotational parameter and electric charge of the BH, respectively. When $Q = 0$, this metric reduces to the Kerr solution; when $a = 0$, it reduces to the RN metric; and when $Q = a = 0$ it further reduces to the Schwarzschild metric. The angular momentum of the BH is given by $J = Ma$. The equation $\Delta = 0$ has two roots, namely $r_\pm = M \pm \sqrt{M^2 - (a^2+Q^2)}$. Here r_+ corresponds to the event horizon, while r_- represents the inner horizon. The surface gravity is

$$\kappa = \frac{\sqrt{M^2 - a^2 - Q^2}}{r_+^2 + a^2}. \tag{2.4}$$

When the inner and outer event horizons coincide, its surface gravity vanishes, which implies that the BH exists in a zero temperature state. Under such circumstances, the equation $M^2 = a^2 + Q^2$ holds.

We now turn our attention to the motion of a test particle endowed with both spin and charge in the Kerr–Newman spacetime. Unlike a non-spinning test particle whose motion adheres to the geodesic equations, the dynamics of the spinning test particle are governed by the Mathisson–Papapetrou–Dixon (MPD) equations [46],

$$\frac{Dp^\mu}{D\tau} = -\frac{1}{2}R^\mu_{\nu\alpha\beta}u^\nu S^{\alpha\beta} - mqF^\mu_\nu u^\nu, \tag{2.5}$$

$$\frac{DS^{\mu\nu}}{D\tau} = p^\mu u^\nu - u^\mu p^\nu. \tag{2.6}$$

Here, $D/D\tau$ represents the covariant derivative along the particle's trajectory, where τ is the affine parameter of the orbit. The four-momentum is denoted by p^μ, the four-velocity by u^ν, and the spin tensor of the particle by $S^{\mu\nu}$. The mass and charge of the particle are m and q, respectively, and F^μ_ν signifies the electromagnetic field tensor of the spacetime. In general, the four-velocity and four-momentum are non-parallel; that is, there exists a deviation between the kinematic velocity and the dynamical momentum. This deviation stems from the coupling effects of the particle's spin with the spacetime curvature and the electromagnetic field. To precisely relate the four-velocity and the four-momentum, a spin supplementary condition must be imposed. In this study, we adopt the Tulczyjew constraint [49,50],

$$S^{\mu\nu}p_\nu = 0. \tag{2.7}$$

This condition sets the time components of the spin tensor to zero in the rest frame of the four-momentum. From this, the normalized four-velocity can be defined as $u^\mu = p^\mu/m$. The mass m and the spin magnitude $\bar{S}$ are two constants of motion of the system, and they are satisfied by $-m^2 = p^\mu p_\mu$ and $2\bar{S}^2 = S^{\mu\nu}S_{\mu\nu}$.

In the Kerr–Newman spacetime, two Killing vectors are present, namely $\xi^\mu = \left(\frac{\partial}{\partial t}\right)^\mu$ and $\phi^\mu = \left(\frac{\partial}{\partial \phi}\right)^\mu$. These Killing vectors correspond to two conserved quantities: the energy E and the angular momentum L, which are given by the following expressions

$$\tilde{E} = \frac{E}{m} = \frac{1}{2m}S^{\mu\nu}\nabla_\nu\xi_\mu - u_\mu\xi^\mu - \tilde{q}A_t, \tag{2.8}$$

$$\tilde{L} = \frac{L}{m} = -\frac{1}{2m}S^{\mu\nu}\nabla_\nu\phi_\mu + u_\mu\phi^\mu + \tilde{q}A_\phi, \tag{2.9}$$

and the parameter $\tilde{q} = \frac{q}{m}$. When the particle traverses the equatorial plane of this BH, its spin vector remains perpendicular to the orbital plane. In other words, the spin vector possesses a non-zero component solely along the polar axis. Under such a condition, the non-vanishing coordinate components of the spin tensor can be formulated as follows

$$S^{r\phi} = -S^{\phi r} = -\frac{\tilde{S}}{r}p_t, \quad S^{rt} = -S^{tr} = \frac{\tilde{S}}{r}p_\phi,$$
$$S^{\phi t} = -S^{t\phi} = -\frac{\tilde{S}}{r}p_r. \tag{2.10}$$

Here, $\tilde{S}$ represents the reduced spin parameter; that is, $\tilde{S} = \frac{\bar{S}}{m}$. The quantities p_t, p_r, and p_ϕ are the covariant components of the four-momentum. These covariant components are related to their contravariant counterparts through the metric.

The explicit expressions for the four-momentum and four-velocity of the spinning charged particle are presented in [46]. In this paper, we directly employ these results to calculate the exponent. The coordinate components of the particle's normalized four-momentum are given by

$$\begin{aligned} p^t = \frac{1}{\Sigma_0 \Xi}\Big[&\tilde{E}r^6 - \tilde{q}Qr^5 + a^2\tilde{E}r^4 \\ &+r^3(2a^2\tilde{E}M - 2a\tilde{L}M - a^2\tilde{q}Q + 3a\tilde{E}M\tilde{S} \\ &-\tilde{L}M\tilde{S}) + r^2(-a^2\tilde{E}Q^2 + a\tilde{L}Q^2 - 2aM\tilde{q}Q\tilde{S} \\ &-2a\tilde{E}Q^2\tilde{S} + \tilde{L}Q^2\tilde{S}) \\ &+r(a^3\tilde{E}M\tilde{S} - a^2\tilde{L}M\tilde{S} \\ &+a\tilde{q}Q^3\tilde{S}) + a^2\tilde{L}Q^2\tilde{S} - a^3\tilde{E}Q^2\tilde{S}\Big], \end{aligned} \tag{2.11}$$

$$\begin{aligned} p^\phi = \frac{1}{\Sigma_0 \Xi}\Big[&r^4(\tilde{L} - \tilde{E}\tilde{S}) \\ &+r^3(2a\tilde{E}M - 2\tilde{L}M - a\tilde{q}Q + 2\tilde{E}M\tilde{S} + \tilde{q}Q\tilde{S}) \\ &+r^2(-a\tilde{E}Q^2 + \tilde{L}Q^2 - 2M\tilde{q}Q\tilde{S} \\ &-\tilde{E}Q^2\tilde{S}) + r(a^2\tilde{E}M\tilde{S} - a\tilde{L}M\tilde{S} \\ &+\tilde{q}Q^3\tilde{S}) + a\tilde{L}Q^2\tilde{S} - a^2\tilde{E}Q^2\tilde{S}\Big], \end{aligned} \tag{2.12}$$

$$\begin{aligned} p^r = \pm\frac{1}{r\Xi}\Big[&r^6\Big(-(a\tilde{E} - \tilde{L})^2Q^2 \\ &+2(a\tilde{E} - \tilde{L})(a\tilde{E}M - \tilde{L}M - a\tilde{q}Q)r \\ &+\big(a^2(-1 + \tilde{E}^2) - \tilde{L}^2 \\ &+(-1 + \tilde{q}^2)Q^2\big)r^2 + 2(M - \tilde{E}\tilde{q}Q)r^3 \\ &+(-1 + \tilde{E}^2)r^4\Big) + 2r^4\Big(2a^2\tilde{E}\tilde{L}(Q^2 - Mr) \\ &+a^3\tilde{E}^2(-Q^2 + Mr) \\ &+\tilde{L}r(-\tilde{q}Q + \tilde{E}r)(2Q^2 + r(-3M + r)) \\ &+a\big(\tilde{L}^2(-Q^2 + Mr) \\ &+r(\tilde{q}Q - \tilde{E}r)(2\tilde{E}Q^2 - 3\tilde{E}Mr \\ &+\tilde{q}Qr)\big)\Big)\tilde{S} + r^2\Big(\tilde{L}^2(Q^2 - Mr)^2 \\ &-r^2(Q^2 - 2Mr + r^2)\big((2 + \tilde{q}^2)Q^2 \\ &-2(M + \tilde{E}\tilde{q}Q)r + \tilde{E}^2r^2\big) \\ &-2a\tilde{L}(Q^2 - Mr)\big(\tilde{q}Qr + \tilde{E}(Q^2 - r(M + r))\big) \\ &+a^2(Q^2 - Mr)\big(2\tilde{E}\tilde{q}Qr - 2r^2 \\ &+\tilde{E}^2(Q^2 - r(M + 2r))\big)\Big)\tilde{S}^2 \\ &-(Q^2 - Mr)^2\big(a^2 + Q^2 + r(-2M + r)\big)\tilde{S}^4\Big]^{1/2}. \end{aligned} \tag{2.13}$$

In the above equations, Σ_0 and Ξ are defined as

$$\Sigma_0 = a^2 + Q^2 - 2Mr + r^2, \quad \Xi = r^4 + Q^2\tilde{S}^2 - Mr\tilde{S}^2, \tag{2.14}$$

the symbols "+" and "−" serve to indicate the direction of the particle's radial motion. More precisely, "+" corresponds to outward radial motion, whereas "−" indicates inward radial motion. Consequently, the normalized four-velocity of the particle is expressed as

$$\begin{aligned} \frac{dt}{d\tau} = \frac{1}{r^2}\Big[&\Big(\big(a^2 + r^2\big)A - a^2B\Big)p^t \\ &+a\left(a^2 + r^2\right)(B - A)p^\phi - aCr\Big], \end{aligned} \tag{2.15}$$

$$\frac{d\phi}{d\tau} = \frac{1}{r^2}\Big[a(A - B)p^t + \Big(\big(a^2 + r^2\big)B - a^2A\Big)p^\phi - Cr\Big], \tag{2.16}$$

$$\frac{dr}{d\tau} = Ap^r, \tag{2.17}$$

with

$$A = \frac{r^4 + \tilde{S}^2\left(Q^2 - Mr\right)}{K}, \quad B = \frac{r^4 + 2Mr\tilde{S}^2 - 3Q^2\tilde{S}^2}{K},$$
$$C = \frac{qQr^2\tilde{S}}{K}, \tag{2.18}$$

where K is given by

$$K = k^2\left(4\tilde{S}^2Q^2 - 3Mr\right) + \tilde{q}Qr^2\tilde{S}k/m + \tilde{S}^2\left(Q^2 - Mr\right) + r^4, \tag{2.19}$$

and k is

$$k = \frac{r^3(\tilde{L} - \tilde{E}a - \tilde{E}\tilde{S}) + r^2\tilde{q}Q\tilde{S}}{\Xi}. \tag{2.20}$$

In the context of BH phase transitions, the functional dependence of the proper-time LE and coordinate-time LE on temperature has been utilized to characterize phase transitions. For a chaotic particle motion, the divergence of trajectories is governed solely by the underlying system dynamics, independent of whether time is measured in terms of proper time or coordinate time. Consequently, the introduction of distinct exponents for proper time and coordinate time is unnecessary for chaos bound detection. For simplicity and computational efficiency, we express the radial equation of motion as the derivative of the particle's radial coordinate with respect to coordinate time, which is

$$\dot{r} = \frac{dr}{dt} = \frac{Ar^2 p^r}{\left(\left(a^2+r^2\right)A - a^2 B\right)p^t + a\left(a^2+r^2\right)(B-A)p^\phi - aCr}. \tag{2.21}$$

Given that the present work is concerned exclusively with the exponent characterizing radial trajectory deviation of the particle, the angular components of the equations of motion – specifically, those involving derivatives with respect to coordinate time – are not presented in this analysis.

3 LEs in Kerr–Newman spacetimes

3.1 LEs

Currently, a considerable number of works have addressed the derivation of LEs [51–54]. In [53], the authors successfully established a correlation between the exponents and the second derivative of the effective potential governing the radial motion of particles. Extending this framework, we now derive the exponent governing the chaotic dynamics of spinning particles. Our analysis commences with the radial equation of motion for the particle,

$$\frac{1}{2}m\dot{r}^2 + \mathcal{V}_{\text{eff}} = 0, \tag{3.1}$$

where $\mathcal{V}_{\text{eff}}$ denotes the effective potential, and it can be written as $\mathcal{V}_{\text{eff}} = -\frac{1}{2}m\dot{r}^2$. The radial motion is governed by Eq. (2.21). The local maximum of this potential corresponds to the unstable equilibrium orbit r_0 of the particle, which is obtained by solving $\mathcal{V}'_{\text{eff}} = 0$ together with $\mathcal{V}''_{\text{eff}} < 0$. To analyze small perturbations around this maximum, the orbit is expressed as $r(t) = r_0 + \epsilon(t)$, where $\epsilon(t)$ represents a small disturbance. Substituting this into Eq. (3.1) and expanding the effective potential around r_0 yield a linearized equation for ϵ,

$$\frac{1}{2}m\dot{\epsilon}^2 + V_{\text{eff}}(r_0) + \frac{1}{2}V''_{\text{eff}}(r_0)\,\epsilon^2 + \mathcal{O}(\epsilon) \simeq 0, \tag{3.2}$$

where $\mathcal{O}(\epsilon)$ and $V_{\text{eff}}(r_0)$ are higher order and constant terms, respectively. The former terms can be neglected, whereas the latter can be eliminated by redefining the zero point of the potential. This equation admits an exponential solution $\epsilon \propto e^{\pm\lambda t}$, with the LE λ defined by [28,54]

$$\lambda^2 = -\frac{\mathcal{V}''_{\text{eff}}(r_0)}{m}. \tag{3.3}$$

If $\lambda^2 > 0$, the orbit exhibits instability – a hallmark of chaotic motion. Conversely, the orbit remains stable when $\lambda^2 < 0$. By comparing λ with the BH surface gravity κ, one can assess whether the exponent is larger than the MSS scale.

3.2 LEs in the non-extremal spacetime

In this subsection, we numerically calculate the exponents for chaos of the charged particle in the Kerr–Newman spacetime and the BH surface gravity. We first define a directional spin $S = \pm\bar{S}$, where the positive sign denotes alignment with the z-axis, while the negative sign indicates opposition to this axis. Similarly, the signs of the BH angular momentum J and the particle's total angular momentum $\tilde{L}$ indicate alignment with or opposition to the z-axis, respectively. In all subsequent calculations, we work in units where $M = m = 1$ for simplicity, such that the particle's angular momentum $L = \tilde{L}$, its charge $q = \tilde{q}$, and its spin magnitude $\bar{S} = \tilde{S}$. Unless otherwise specified, we fix the BH parameters as $|J| = 0.22$ and $Q = 0.90$, with the particle charge set to $q = 0.10$.

We commence our analysis by calculating the effective potential of the particle. Figure 1 displays the radial dependence of this effective potential, where the maximum corresponds to the position of the unstable circular orbit. Our results demonstrate that, compared to the spinless case, the spin significantly alters the extremal structure of the potential. For the spin anti-aligned with the z-axis, the potential maximum shifts outward, indicating an increase in the radius of the unstable equilibrium orbit. Conversely, for the aligned spin, the maximum shifts inward, leading to a reduced orbital radius. This reveals that the spin orientation directly alters the particle's equilibrium position in the equatorial plane, potentially influencing the orbital stability and the exponent. Based on these findings, we use Eqs. (2.4), (2.11)–(2.14), (2.18), and (2.19)–(2.21) in conjunction with Eq. (3.3) to calculate the exponents and the surface gravity, and to systematically investigate the upper bound of the LEs in the subsequent analysis. The results are presented in Figs. 2, 3, 4 and 5. If $\lambda > \kappa$, the exponents exceed the MSS scale; otherwise, they fall below it.

As shown in Fig. 2, when the BH angular momentum is anti-aligned with the z-axis, the difference between the exponents and the surface gravity first decreases with increasing angular momentum before transitioning to monotonic growth. Once the angular momentum exceeds a critical threshold, the exponent surpasses the surface gravity. Conversely, when the BH spin is aligned with the z-axis, the difference rises monotonically with increasing angular momentum, ultimately crossing the zero line and leading to the exponent exceeding the MSS scale. A direct comparison of the particle spin orientations reveals that anti-aligned spins correspond to larger thresholds, whereas aligned spins yield

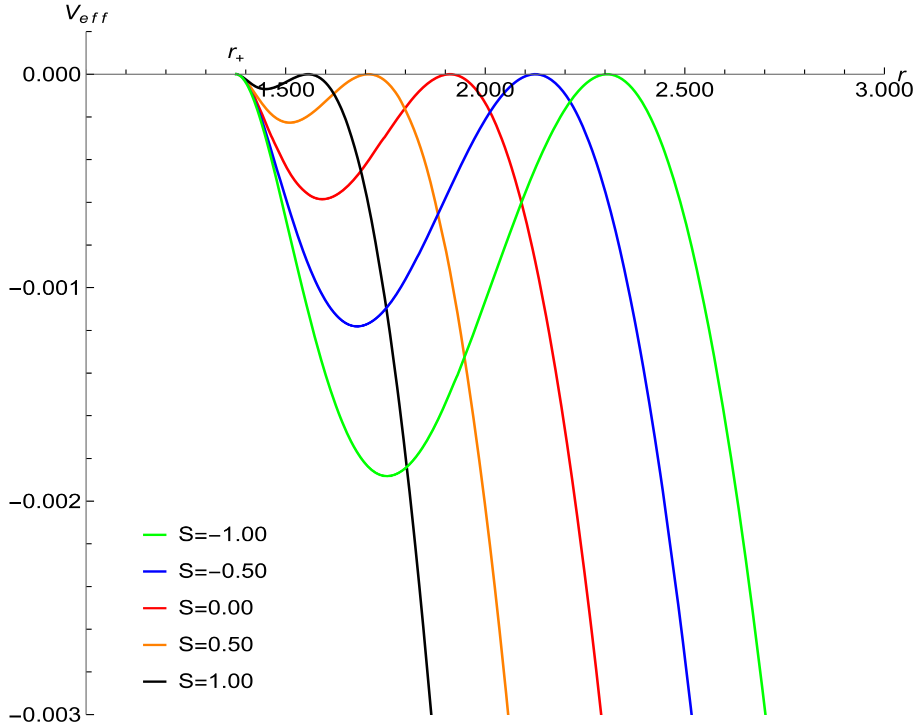

Fig. 1 Curves show the variation of the effective potential of the charged particle with its radius, calculated with $J = 0.22$ and $L = 20.00$

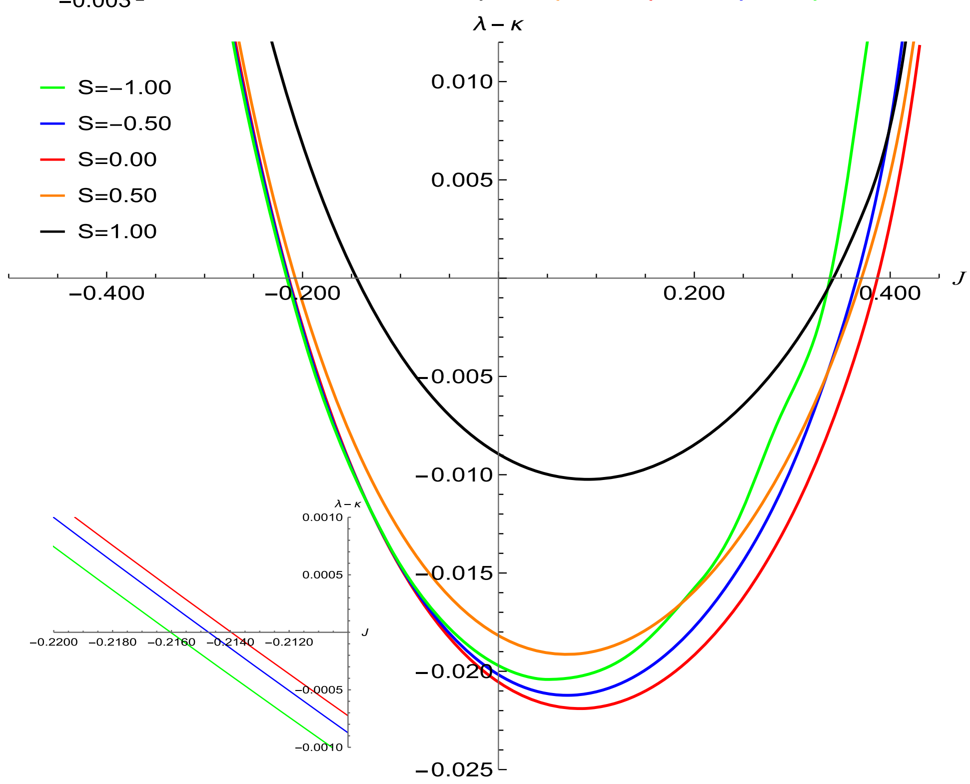

Fig. 2 Curves displays the difference between the exponent and the surface gravity as a function of the BH's angular momentum, calculated with the parameters fixed as $L = 20.00$

smaller critical values. This result confirms that, when the BH spin is aligned with the z-axis, the anti-aligned particle spins most readily cause the exponent to exceed the MSS scale.

In Fig. 3, we analyze the influence of particle spin on the exponents. When the BH rotates in the same direction as the z-axis, the exponents are consistently smaller than the surface gravity. We therefore focus on the scenario in which the BH rotates in the opposite direction to the z-axis, as shown in Fig. 3b. In Fig. 3b, when the particle spin is aligned with the z-axis, the exponents increase with the spin magnitude. Once the spin magnitude exceeds certain thresholds, the exponents surpass the surface gravity. For small spin magnitudes ($S \leq 0.50$), the exponents grow slowly; when the

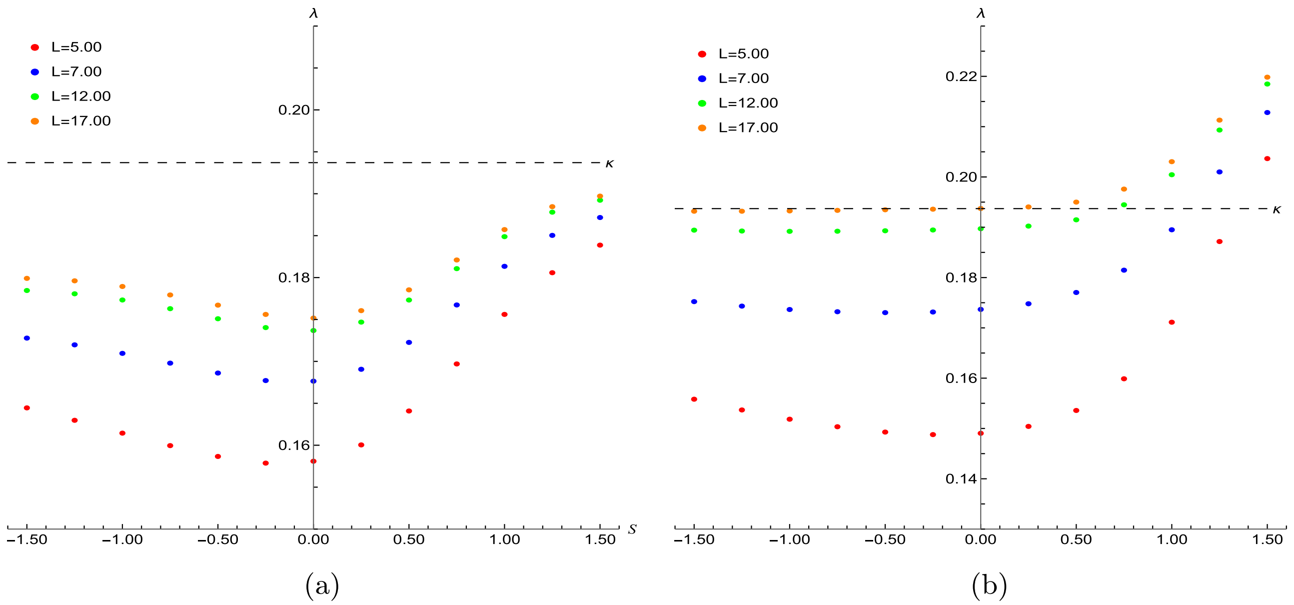

Fig. 3 LEs are shown as a function of the particle spin. Panels **a** and **b** depict the configurations where the BH's rotational axis is aligned with and anti-parallel to the z-axis, respectively

spin magnitude exceeds this threshold, they increase rapidly. This indicates that a larger spin magnitude enhances chaotic instability, making it more likely for the exponents to exceed the MSS scale. When the particle spin is anti-aligned with the z-axis, the exponents vary slowly with increasing spin magnitude. For a small total angular momentum of the particle (e.g., $L = 5.00$), the exponent first decreases and then increases as the spin magnitude grows.

Figure 4 shows the variation of the exponents with the particle's total angular momentum. This figure also indicates that the exponents are consistently smaller than the surface gravity when the BH rotates in the same direction as the z-axis. From Fig. 4a, we observe that for a particle with a large total angular momentum, a greater spin magnitude corresponds to a larger LE. However, at the same spin magnitude, the exponent is larger when the particle spin is aligned with the z-axis than when it is anti-aligned with the z-axis. In Fig. 4b, it can be observed that the exponents for all spin configurations increase monotonically with the total angular momentum, though the growth rate slows down at the large angular momenta. The exponents are larger than the surface gravity when the angular momentum exceeds a critical threshold. For a fixed spin magnitude, the exponent of the aligned spin particle is consistently higher than that of the anti-aligned particle, indicating a stronger exponential sensitivity to initial conditions. Consequently, the critical angular momentum threshold is smaller for the anti-aligned spin, confirming that the anti-aligned configuration more readily causes the exponents to exceed the surface gravity compared to the aligned case.

Figure 5 presents the variation of exponents with the particle charge. It is observed that as the particle charge increases from negative to positive values, the exponents for all spin states exhibit an upward trend. This indicates that an increase in negative charge suppresses chaotic behavior, while an increase in positive charge enhances it. When the BH's rotation direction is aligned with the z-axis, the exponents remain consistently smaller than the surface gravity. In contrast, when the BH rotates in the opposite direction to the z-axis, near $q < -1.10$, the particle with spins aligned with the z-axis and large spin magnitudes exhibit the fastest growth rate of the exponent. As the particle charge increases from negative to positive, the exponent of particle with $S = -1$ first exceeds the surface gravity; for the particle with other spin states, their exponents sequentially surpass the charge threshold, subsequently causing the exponents to exceed the MSS scale. Therefore, compared to gravitational electromagnetic interactions, repulsive electromagnetic effects exhibit a higher sensitivity to chaotic behavior.

Figures 3, 4 and 5 indicate that when the BH rotation direction is aligned with the z-axis, the exponents remain consistently smaller than the surface gravity under the specific parameter conditions considered. This behavior can be attributed to the relatively small values of the relevant BH and particle parameters. However, when these parameters take sufficiently large values, the exponents can exceed the surface gravity, as illustrated in Fig. 2. A detailed discussion of this scenario is presented in the following section.

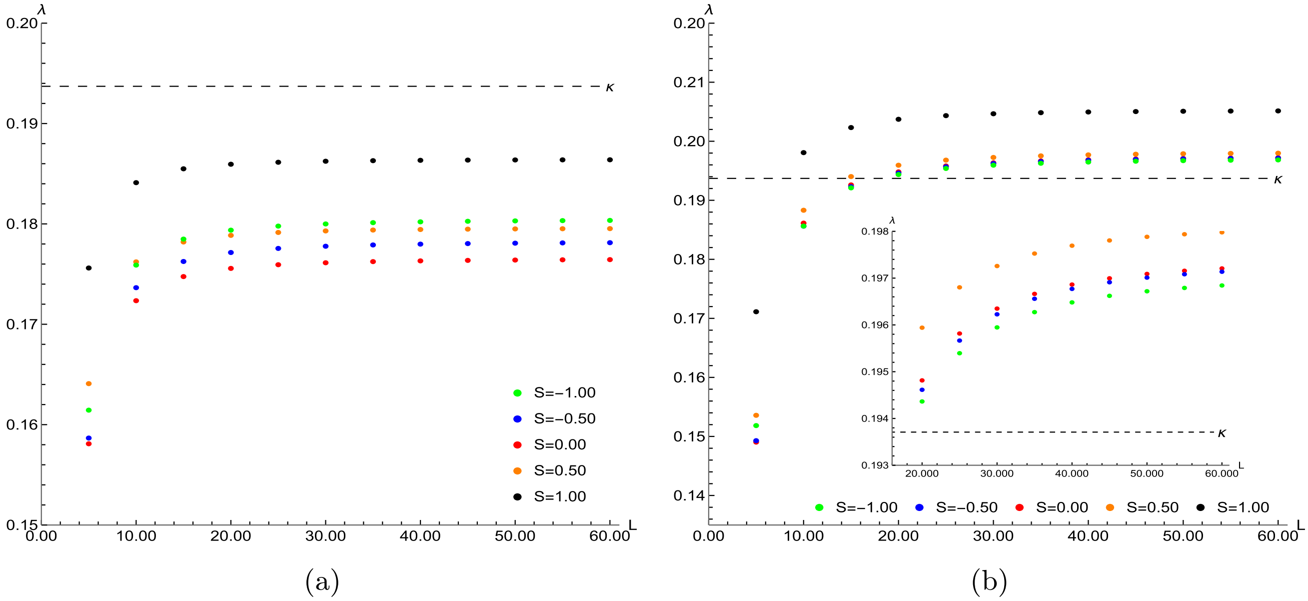

Fig. 4 LEs for chaos of the charged particle varies with its total angular momentum. Panels **a** and **b** depict the configurations where the BH's rotational axis is aligned with and anti-parallel to the z-axis, respectively

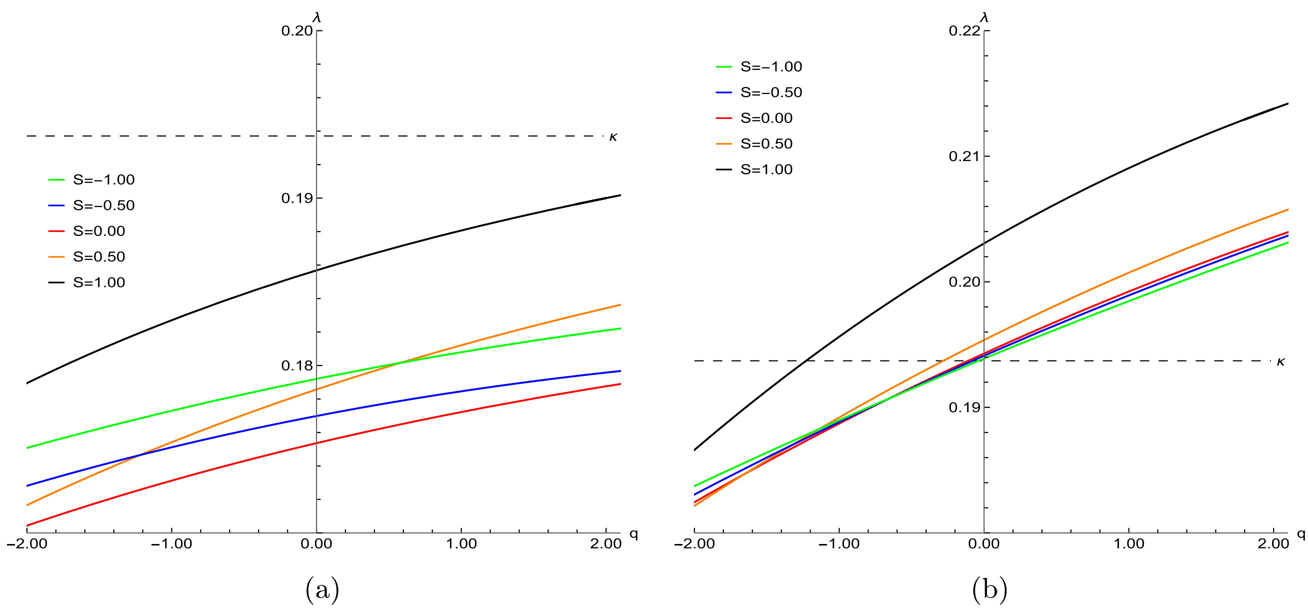

Fig. 5 Curves shows the variation of the LEs for the chaotic particle with respect to its charge, calculated with the parameters fixed as $L = 20.00$. Panels **a** and **b** depict the configurations where the BH's rotational axis is aligned with and anti-parallel to the z-axis, respectively

3.3 LEs in the extremal spacetimes

When the BH approaches an extremal configuration, its Hawking temperature and surface gravity vanish, reducing the spacetime to a zero-temperature state. We study the upper bound of the exponents in this limiting case. Since the surface gravity vanishes, violation occurs if $\lambda > 0$. For an extreme Kerr–Newman BH, the constraint $a^2 + Q^2 = 1$ holds by definition. We fix $Q^2 = 0.75$, $J^2 = 0.25$ and $q = 0.10$, and then calculate the exponents in this spacetime. At this point, since no equilibrium orbit exists when the BH's rotation direction is aligned with the z-axis, we restrict our discussion to the case where the two directions are opposite. The resulting plot is shown in Fig. 6.

From panel Fig. 6a, we observe that all exponents take positive values in this zero-temperature system. When the particle spin is aligned with the z-axis, for a low angular momentum (e.g., $L = 5.00$), the exponent increases monotonically

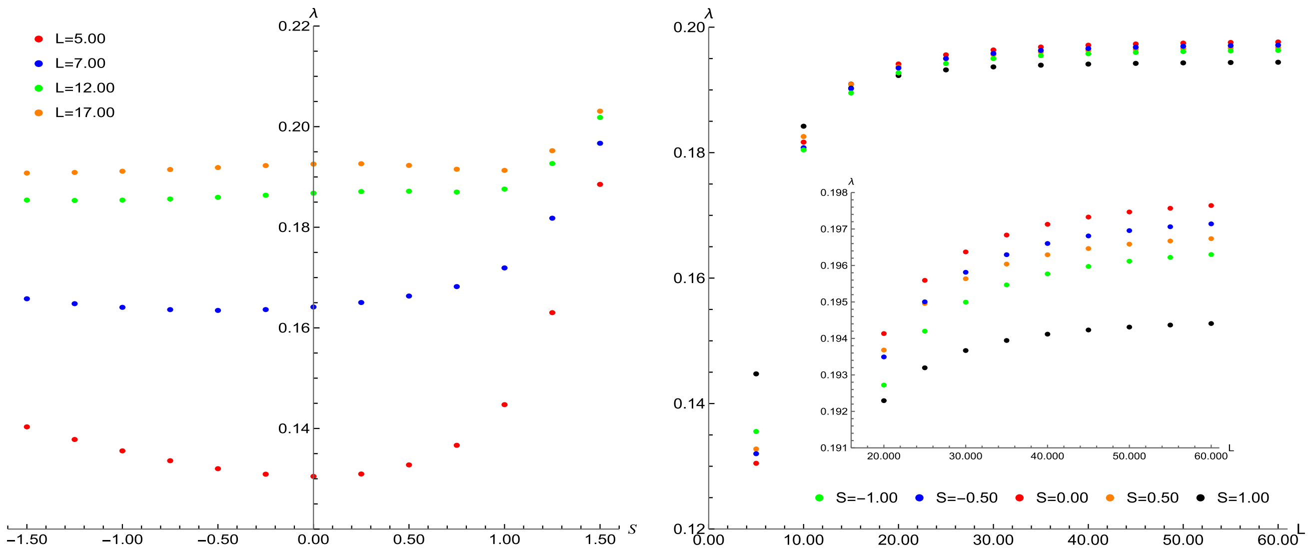

(a) (b)

Fig. 6 Variations of the LEs of the chaotic charged particle in the extremal Kerr–Newman spacetime with respect to the particle spin and angular momentum, corresponding to panels **a** and **b**, respectively

with the spin magnitude. For a sufficiently large total angular momentum (e.g., $L = 17.00$), the exponent exhibits a non-monotonic trend, decreasing first and then increasing. When the particle spin is anti-aligned with the z-axis, the dependence of the exponent on the spin magnitude is sensitive to the total angular momentum of the particle. From panel Fig. 6b, it is evident that all exponents exceed the surface gravity. The exponent corresponding to each spin increases monotonically with the total angular momentum, and the growth rate slows down significantly in the large angular momentum regime. However, the value of the exponent for the particle with large spin magnitude is notably smaller than that for the spinless case. This behavior differs from that observed in the non-extremal spacetime. This finding suggests that the zero-temperature spacetime can suppress the chaotic dynamics of spinning particles, in contrast to the non-extremal case where anti-aligned spins typically enhance chaos.

When $Q = 0.00$ and $a = 1.00$, the extremal Kerr–Newman BH is reduced to an extremal Kerr BH. Panel Fig. 7a presents the exponents as a function of the particle spin in this spacetime. When the spin is anti-aligned with the z-axis, for large total angular momenta $L = 12$ and $L = 17$, the exponents increase slowly as the anti-parallel spin magnitude approaches zero, indicating that a larger anti-parallel spin exerts a suppressive effect on chaos. For $L = 5.00$, the exponent decreases markedly as the spin orientation transitions from anti-parallel to parallel, whereas for $L = 7.00$ this variation is relatively weak. When the spin is aligned with the z-axis, the exponents decrease monotonically with increasing parallel spin magnitude, with the reduction becoming more pronounced at larger spin magnitudes. This demonstrates that the particle spin parallel to the z-axis weakens the chaotic instability. Panel Fig. 7b shows the exponents as a function of the total angular momentum. For all spin orientations, the exponents increase monotonically with increasing the total angular momentum, indicating that a larger total angular momentum enhances the instability of chaos. The growth is more rapid in the small angular momentum regime, while the growth rate diminishes significantly and gradually approaches a slow increase as the angular momentum becomes larger. The inset provides a detailed view of the range $20 < L < 60$, where the exponents continues to rise slowly with the angular momentum, but the differences among spin configurations become more pronounced. Specifically, the exponent for the spinless particle is relatively large, whereas the particle with large spin parallel to the z-axis exhibits the smallest exponent, confirming that a large parallel spin magnitude suppresses chaotic behavior. Overall, the total angular momentum enhances chaos, while the spin orientation and magnitude modulate this enhancement.

When $a = 0.0$ and $Q = 1.00$, the extremal Kerr–Newman BH is reduced to an extremal RN BH. Panel Fig. 8a displays the exponents as a function of the particle spin in this spacetime. All exponents are positive, signifying that these exponents are larger than the MSS scale. The influence of the spin on the exponents exhibits a clear directional dependence. When the spin is anti-parallel to the z-axis, the exponents decrease slowly as the anti-parallel spin magnitude diminishes. In contrast, when the spin is parallel to the z-axis, the exponents increase significantly with increasing parallel spin magnitude, with the growth being particularly pronounced in the large spin regime. This indicates that the

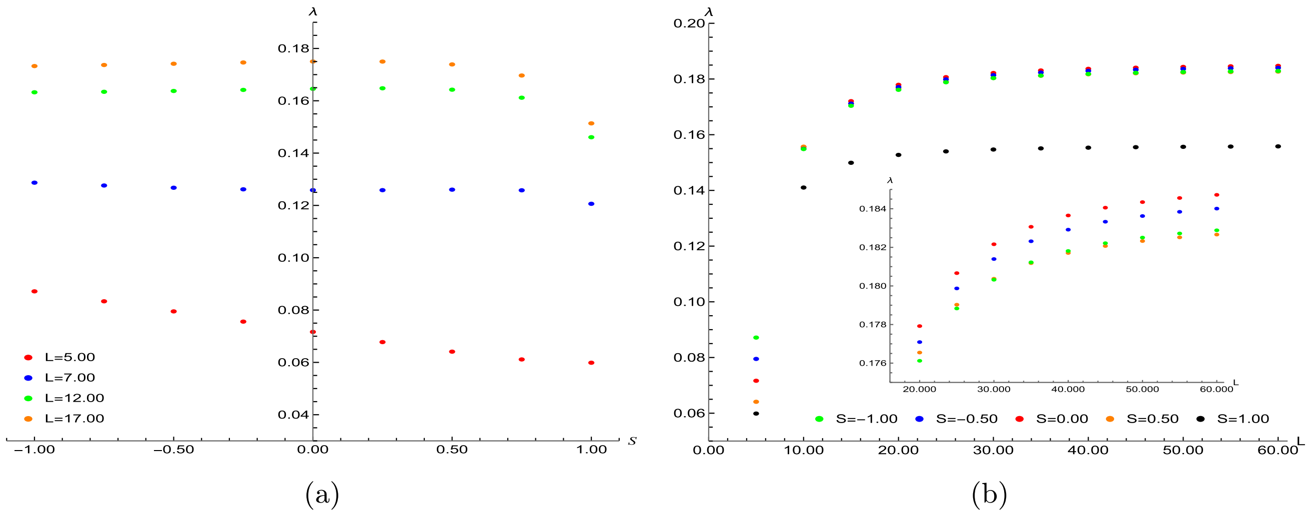

Fig. 7 Variations of the LE of the chaotic charged particle in the extremal Kerr spacetime with respect to the particle spin and angular momentum, corresponding to panels **a** and **b**, respectively

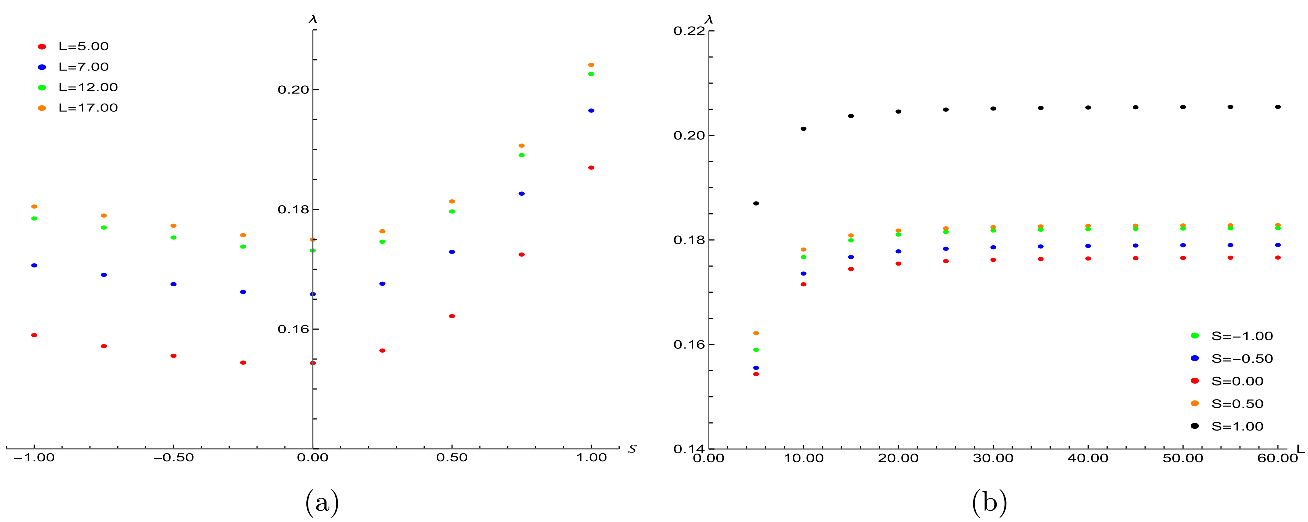

Fig. 8 Variations of the LE of the chaotic charged particle in the extremal RN spacetime with respect to the particle spin and angular momentum, corresponding to panels **a** and **b**, respectively

parallel spin substantially enhances the chaotic behavior of the particle. In panel Fig. 8b, the exponents increase monotonically with the total angular momentum, demonstrating that a larger total angular momentum amplifies the instability of chaos. Notable differences are also observed among spin configurations: the particle with large spin parallel to the z-axis consistently exhibit the largest exponent, the spinless particle yields a relatively lower exponent, and the particle with anti-parallel spin lie in between. In summary, in this spacetime, both the total angular momentum and the particle spin enhance the chaotic instability.

4 Conclusions and discussions

In this work, we investigated the LEs characterizing the chaotic dynamics of spinning charged particle in the Kerr–Newman spacetime, and found that these exponents can exceed the surface gravity of the BH. Specifically, in the non-extremal Kerr–Newman spacetime, when the BH rotates in the same direction as the z-axis, the phenomenon that the exponents exceed the surface gravity occurs only when the BH angular momentum surpasses a threshold. Varying the particle's spin, total angular momentum, or charge does not give rise to any violation. A reasonable explanation is that the values of the parameters related to the BH and particle are not large enough, rendering the centrifugal force or the electromagnetic interaction insufficiently strong. When these forces become sufficiently large, these exponents can exceed the surface gravity. In contrast, when the BH rotates in the opposite direction to the z-axis, the violations emerge once the BH angular momentum, or the particle's spin, total angular momentum, or charge exceeds their respective thresholds. This finding establishes that the rotation direction of the BH exerts a more decisive influence on the relation between the exponents and the surface gravity. We further found that the sign of the particle's charge exerts a markedly asymmetric effect on chaos: an increase in the negative charge of the particle suppresses chaos, whereas an increase in the positive charge enhances it. When the BH is in an extreme state, the system transforms into a zero-temperature system. Under this extremal condition, we extended our analysis to the Kerr–Newman, RN, and Kerr spacetimes. The results indicate that, for all spins, the exponents are positive.

Our numerical framework assumes comparable particle and BH masses for mathematical tractability [33–36,55–57]. However, in astrophysically relevant scenarios, test particles typically have masses significantly smaller than that of the BH. Moreover, this study has not yet incorporated the back-reaction effect of the particle on the background spacetimes. Only by taking this factor into account can an accurate determination be made regarding whether the exponents are larger than the MSS scale.

Funding This work is supported by the NSFC (Grant No. 12105031) and Tianfu talent project.

Data Availability Statement This manuscript has no associated data. [Author's comment: This is a theoretical research, and no experimental data has been listed.]

Code Availability Statement This manuscript has no associated code/software. [Author's comment: The points in Figs. 1-8 were generated using a Mathematica program which is available from the authors upon request.]

References

1. P. Pradhan, Stability analysis and quasinormal modes of Reissner–Nordstrom space-time via Lyapunov exponent. Pramana **87**, 5 (2016)
2. R.A. Jalabert, H.M. Pastawski, Environment-independent decoherence rate in classically chaotic systems. Phys. Rev. Lett. **86**, 2490 (2001)
3. S.H. Shenker, D. Stanford, Multiple shocks. JHEP **1412**, 046 (2014)
4. S.H. Shenker, D. Stanford, Black holes and the butterfly effect. JHEP **1403**, 067 (2014)
5. D.A. Roberts, D. Stanford, L. Susskind, Localized shocks. JHEP **03**, 051 (2015)
6. A. Avdoshkin, A. Dymarsky, Euclidean operator growth and quantum chaos. Phys. Rev. Res. **2**, 043234 (2020)
7. S.H. Shenker, D. Stanford, Stringy effects in scrambling. JHEP **1505**, 132 (2015)
8. V. Jahnkea, K.Y. Kim, J. Yoon, On the chaos bound in rotating black holes. JHEP **1905**, 037 (2019)
9. E.B. Rozenbaum, S. Ganeshan, V. Galitski, Lyapunov exponent and out-of-time ordered correlator's growth rate in a chaotic system. Phys. Rev. Lett. **118**, 086801 (2017)
10. T. Xu, T. Scaffidi, X. Cao, Does scrambling equal chaos? Phys. Rev. Lett. **124**, 140602 (2020)
11. T. Xu, T. Scaffidi, X. Cao, Refined quantum Lyapunov exponents from replica out-of-time-order correlators. Phys. Rev. D **108**, 105023 (2023)
12. J. Maldacena, S.H. Shenker, D. Stanford, A bound on chaos. JHEP **1608**, 106 (2016)
13. J.M. Maldacena, The Large N limit of superconformal field theories and supergravity. Adv. Theor. Math. Phys. **2**, 231 (1998)
14. E. Witten, Anti-de Sitter space and holography. Adv. Theor. Math. Phys. **2**, 253 (1998)
15. J. Maldacena, D. Stanford, Remarks on the Sachdev–Ye–Kitaev model. Phys. Rev. D **94**, 106002 (2016)
16. S. Sachdev, J. Ye, Gapless spin-fluid ground state in a random quantum Heisenberg magnet. Phys. Rev. Lett. **70**, 3339 (1993)
17. A. Kitaev, Hidden correlations in the hawking radiation and thermal noise, talk given at *Fundamental Physics Prize Symposium*, November 10, 2014
18. A. Kitaev, A simple model of quantum holography, talk at *KITP* (2015)
19. X.L. Han, Z.D. Yu, Quantum chaos of the Bose–Fermi Kondo model at the intermediate temperature. Phys. Rev. B **104**, 085139 (2021)
20. B. Craps, S. Khetrapal, C. Rabideau, Chaos in CFT dual to rotating BTZ. JHEP **2111**, 105 (2020)
21. M. Blake, H. Liu, On systems of maximal quantum chaos. JHEP **2105**, 229 (2021)
22. K. Hashimoto, N. Tanahashi, Universality in chaos of particle motion near black hole horizon. Phys. Rev. D **95**, 024007 (2017)
23. Q.Q. Zhao, Y.Z. Li, H. Lü, Static equilibria of charged particles around charged black holes: chaos bound and its violations. Phys. Rev. D **98**, 124001 (2018)
24. Y.Q. Lei, X.H. Ge, Circular motion of charged particles near charged black hole. Phys. Rev. D **105**, 084011 (2022)
25. Y.Q. Lei, X.H. Ge, C. Ran, Chaos of particle motion near a black hole with quasitopological electromagnetism. Phys. Rev. D **104**, 046020 (2021)
26. Y.Q. Lei, X.H. Ge, S. Dalui, Thermodynamic stability versus chaos bound violation in D-dimensional RN black holes: angular momentum effects and phase transitions. Phys. Lett. B **856**, 138929 (2024)

27. J. Xie, J. Wang, B. Tang, Circular motion and chaos bound of a charged particle near charged 4D Einstein–Gauss–Bonnet–AdS black holes. Phys. Dark Universe **42**, 101271 (2023)
28. S. Jeong, B.H. Lee, H. Lee, W. Lee, Homoclinic orbit and the violation of the chaos bound around a black hole with anisotropic matter fields. Phys. Rev. D **107**, 104037 (2023)
29. K. Li, D.Z. Ma, Z.M. Xu, Chaotic dynamics of string around the charged Kiselev black hole. Phys. Lett. B **860**, 139164 (2025)
30. P. Dutta, K.L. Panigrahi, B. Singh, Chaos bound and its violation in black p-brane. JHEP **2501**, 1 (2025)
31. T.V. Targema, K. Bamba, R. Ali, U. Zafar, Physical constraints on the MSS chaos-bound in black hole spacetimes. Phys. Rev. D **113**, 104056 (2026)
32. C.H. Gao, D.Y. Chen, C.Y. Yu, P. Wang, Chaos bound and its violation in charged Kiselev black hole. Phys. Lett. B **833**, 137343 (2022)
33. N. Kan, B. Gwak, Bound on the Lyapunov exponent in Kerr–Newman black holes via a charged particle. Phys. Rev. D **105**, 026006 (2022)
34. J. Park, B. Gwak, Bound on Lyapunov exponent in Kerr–Newman–de Sitter black holes by a charged particle. JHEP **04**, 023 (2024)
35. B. Gwak, N. Kan, B.H. Lee, H. Lee, Violation of bound on chaos for charged probe in Kerr–Newman–AdS black hole. JHEP **09**, 026 (2022)
36. H. Lee, B. Gwak, Bound on Lyapunov exponent for a charged particle in Kerr–Sen–AdS black hole. Phys. Rev. D **112**, 046018 (2025)
37. D.Y. Chen, C.H. Gao, Angular momentum and chaos bound of charged particles around Einstein–Euler–Heisenberg AdS black holes. New J. Phys. **24**, 123014 (2022)
38. F.H. Lü, J. Tao, P. Wang, Minimal length effects on chaotic motion of particles around black hole horizon. JCAP **1812**, 036 (2018)
39. X.B. Guo, K.K. Liang, B.R. Mu, P. Wang, H.T. Yang, Minimal length effects on motion of a particle in Rindler space. Chin. Phys. C **45**, 023115 (2021)
40. M. Cubrovic, The bound on chaos for closed strings in Anti-de Sitter black hole backgrounds. JHEP **1912**, 150 (2019)
41. K. Hashimoto, K. Sugiura, Causality bounds chaos in geodesic motion. Phys. Rev. D **107**, 066005 (2023)
42. A. Stikonas, Scrambling time from local perturbations of the rotating BTZ black hole. JHEP **1902**, 054 (2019)
43. R.R. Poojary, BTZ dynamics and chaos. JHEP **2003**, 048 (2020)
44. V. Jahnke, K.Y. Kim, J. Yoon, On the chaos bound in rotating black holes. JHEP **1905**, 037 (2019)
45. C. Yang, D.Y. Chen, Y.T. Liu, Motions of spinning particles and chaos bound in Reissner-Nordström spacetime, JHEP **2604**, 205 (2026)
46. R. Hojman, S. Hojman, Spinning charged test particles in a Kerr–Newman background. Phys. Rev. D **15**, 2724 (1977)
47. M. Zhang, W.B. Liu, Innermost stable circular orbits of charged spinning test particles. Phys. Lett. B **789**, 393 (2019)
48. Y.P. Zhang, S.W. Wei, W.D. Guo, T.T. Sui, Y.X. Liu, Innermost stable circular orbit of spinning particle in charged spinning black hole background. Phys. Rev. D **97**, 084056 (2018)
49. W. Tulczyjew, Motion of multipole particles in general relativity theory. Acta Phys. Pol. **18**, 393 (1959)
50. A.J. Hanson, T. Regge, The relativistic spherical top. Ann. Phys. **87**, 498 (1974)
51. P.P. Pradhan, Lyapunov exponent and charged Myers Perry spacetimes. Eur. Phys. J. C **73**, 2477 (2013)
52. P.P. Pradhan, Stability analysis and quasinormal modes of Reissner–Nordstrom space-time via Lyapunov exponent. Pramana **87**, 5 (2016)
53. V. Cardoso, A.S. Miranda, E. Berti, H. Witek, V.T. Zanchin, Geodesic stability, Lyapunov exponents and quasinormal modes. Phys. Rev. D **79**, 064016 (2009)
54. S.Y. Ciou, T. Hsieh, D.S. Lee, Dynamics of spinning particles in Reissner–Nordström black hole exterior. JCAP **05**, 086 (2025)
55. G. Lukes-Gerakopoulos, E. Harms, S. Bernuzzi, A. Nagar, Spinning test-body orbiting around a Kerr black hole: circular dynamics and gravitational-wave fluxes. Phys. Rev. D **96**, 064051 (2017)
56. Y.P. Zhang, S.W. Wei, Y.X. Liu, Spinning test particle in four-dimensional Einstein–Gauss–Bonnet black hole. Universe **6**, 103 (2020)
57. J.M. Ladino, E. Larrañaga, Motion of a spinning particle around an improved rotating black hole, nt. J. Mod. Phys. D **31**, 2250091 (2022)